Beer, A.R., and Lamb, M.P.,2021, Abrasion regimes in fluvial bedrock incision: Geology, v. 49, https://doi.org/10.1130/G48466.1

ADDITIONAL DETAILS ON METHODS

Detailed Methods on the Preparing of the Artificial Sandstone Blocks

We casted mixtures of water, Portland cement and fine sand into boxes of 0.56 * 0.56 * 0.3 m^3 to create homogeneous artificial sandstone of 0.2 mm grainsize, varying the cement to sand ratio for two different tensile strengths σ_t (Sklar and Dietrich, 2001; Table S1). The block's tensile strengths were measured from samples using a Split-Hopkinson pressure bar (Zhou et al., 2011). For the impact abrasion experiments we placed the blocks on sand bags to reduce shacking and confined them with strapped wood boards to avoid shock wave reflection and block cracking from the free lateral surfaces (Fig. 1B). This procedure served as approximation for lateral infinite massive bedrock (i.e. for constant horizontal lithostatic pressure), at least for the relatively small ratios of impactor size to block size of the experiments.

Detailed Methods on Effective Impact Energy Calculation of the Drop Abrasion Experiments

Having vertical and horizontal scale bars attached to the target blocks (Fig. 1B), we tracked the impacting grains by means of a laterally positioned time-laps camera with 100 frames per second, and calculated effective kinetic impact energies, ε_{kin}, responsible for block abrasion:

$$\varepsilon_{kin} = \varepsilon_{imp} - \varepsilon_{reb} = (M_i g H_d) - (\varepsilon_{kin,reb} + \varepsilon_{rot,reb}), \qquad (1)$$

with ε_{imp} being the kinetic impactor energy at the time of impact, ε_{reb} being its rebounding energy afterwards, M_i the impactor mass, g acceleration due to gravity, and H_d the impactor's drop height above the target block (Fig. S1A). Based on time-laps camera observations (Fig. S1B and C), ε_{reb} after the first impact was calculated as the combination of rebound kinetic energy $\varepsilon_{kin,reb}$ and rotational energy $\varepsilon_{rot,reb}$:

$$\varepsilon_{kin,reb} = (M_i g H_{reb}) + \left(0.5 M_i \left(\frac{dx}{dt}\right)^2\right), \qquad (2)$$

$$\varepsilon_{rot,reb} = 0.5M_i \left(\frac{D_i}{2}\right)^2 v_{rot,reb}^2, \qquad (3)$$

with maximum impactor rebound height H_{reb}, first rebound hop distance and time dx and dt, the impactor's rebound rotation velocity $v_{rot,reb}$, and the impactor's diameter D_i (Fig. S1A). We could mostly avoid second impacts on the blocks, but the few happening did neither contribute notable impact energies, nor measurable total abrasion volumes V_a or fragment volumes V_{frag}. Further, we assumed dominance of plastic deformation (abrasion) for the brittle target blocks and neglected any energy loss due to elastic energy radiation (Farin et al., 2015).

Detailed Methods on Total Slab Abrasion Measurements

After each drop experiment and after removing abraded sand and fragments from the target block (Fig. 2A), we placed sub-millimeter-calibrated CHI photogrammetry scale bars (*SfM* bars) on the block's surface, outside the impact area. Then we took five high-resolution photos (42 Megapixels) around and atop the block using a SONY α7RII DSLR camera with a fixed 55 mm lens (Fig. 1B). Applying structure from motion, *SfM*, and multi view stereo photogrammetry in Agisoft Photoscan (Agisoft Photoscan, 2018) resulted in sequential sub-millimeter resolved and accurate digital elevation models, *DEMs*. Vertically differencing these individual epoch *DEMs* in cloudcompare (CloudCompare, 2019), we calculated total abrasion volumes V_a (i.e. the sum of wear and macro-abrasion V_{frag}) for all experiments.

Detailed Methods on Compilation of Single Grain Impact Abrasion Data from the Literature

We compiled published bulk abrasion data from grain drop experiments and from abrasion mill runs (Table S2), all of which didn't report on observed fragment production. For the abrasion mill data, we used an updated version of the total load model (Lamb et al., 2008; neglecting the cover term) to calculate mean effective impact energies, ε_{kin}, and mean eroded volumes, V_a, per single impact in the mills. Thereby, instead of estimating the near-bed volumetric sediment concentration, c_b, from total volumetric sediment flux (Lamb et al., 2008 eq.18), we based its calculation on the known total sediment mass, M_m, in the mills:

$$M_m = \int_0^{H_m} \rho_s \; c(z) \, r_w \, L_c \, dz, \qquad (4)$$

with H_m being the mill's water depth, ρ_s is the grain sediment density, $c(z)$ is the volumetric sediment concentration at height z above the bedrock disk on the mill's bottom, r_w is the total radial width of the bedrock disk, and L_c is the mean circumferential travel distance of a grain in the abrasion mill. By transforming eq. 4 and adopting the thickness of the bedload layer H_b (Sklar and Dietrich, 2004 eq.12), we obtained:

$$\frac{M_m}{\rho_s \, r_w \, L_c} = \; c_b \; \int_0^{H_m} \frac{c(z)}{c_b} \, dz = c_b \; \left[H_b + \int_{H_b}^{H_m} \frac{c(z)}{c_b} \, dz \right], \qquad (5)$$

and hence:

$$c_b = \frac{M_m}{\rho_s \, r_w \, L_c \left[H_b + \int_{H_b}^{H_m} \frac{c(z)}{c_b} \, dz \right]}, \qquad (6)$$

wherein the second term in the square bracket is the Rouse profile (Lamb et al., 2008 eq.26). For the associated Rouse parameter, we used a proportionally constant of 2.5 and a Stokes number of 90 to account for viscous dampening (generally following Scheingross et al., 2014). Mean kinetic impact energies, ε_{kin}, and mean eroded volumes, V_a, of single grain impacts were then calculated as follows:

$$\varepsilon_{kin} = 0.5 M_i \varepsilon_{imp,eff}^2, \tag{7}$$

$$V_a = \frac{V_d}{I_r A_d} = \frac{V_d}{\left(\frac{0.36 c_b\, \varepsilon_{imp,eff}}{V_i}\right) * A_d}, \tag{8}$$

with V_d being the reported total abraded disk volume, I_r is the particle impact rate per disk area, A_d (Lamb et al., 2008 eq.12), V_i is the mean single impacting grain volume, and $\varepsilon_{imp,eff}$ is the effective, vertical grain impact energy accounting for turbulent fluctuations (Lamb et al., 2008 eq.35). Principally, abrasion volume scales with excess impact energy (vertical component of the impact velocity minus a material-specific threshold), but this reduction is neglected here due to generally low thresholds and for the case of mean values for V_a (Neilson, 1968; Engel, 1978; Sklar and Dietrich, 2004).

Detailed Methods on Compilation of Potential Grain Impact Energy in Bedrock Rivers

The potentially median transportable grain size D_{50} (the grainsize of 50% volumetric abundance in a grainsize distribution) for a given river bed slope S and water discharge depths H can be calculated as:

$$D_{50} = \frac{\tau_b}{(\rho_s - \rho_w) g \tau_b^*}, \qquad (9)$$

where ρ_s and ρ_w are the densities of sediment and water, $\tau_b = \rho\ w\ g\ H\ S$ is bed shear stress and τ_b* is its non-dimensional form (the Shields number). The latter value for a bankfull discharge is gained from:

$$\tau_b^* = 1.5\tau_{bc}^* = 0.225\ S^{0.25}, \qquad (10)$$

based on two observations: (i) the general relation between τ_b^* and its critical value τ_{bc}^* for the onset of sediment motion (i.e., the Shields stress; Parker 1978), and (ii) the dependence of τ_{bc}^* on channel slope (Lamb et al., 2008b). Following Lamb et al., 2008, we scaled both volumetric sediment supply (based on Fernandez Luque and van Beek, 1976) and the flow roughness parameter D_{50}, and calculated potential bed impact energies ε_{kin} of D_{50} using the total load model (Lamb et al., 2008; including the sediment cover term), varying both S and H. This procedure presumes this model's validity also for large grain sizes (i.e. valid calculation of bedload layer thickness, bedload transport and settling velocities), and that the grains follow the fluid.

From literature, we compiled a data set on bedrock river sections, comprising riverbed slope S, flow depth H, bedrock type and tensile strength σ_t, and measured grainsizes, as available (Table S3). For cases of not reported σ_t, but descriptions of the local rock type, we adapted σ_t values of comparable rock samples, as measured by Sklar and Dietrich (2001). Reported values of Schmidt Hammer measurements SH were converted to σ_t using the following conversion (Jamshidi et al., 2018):

$$\sigma_t = 0.0347\ 10^6\ SH^{1.3783} \tag{11}$$

Based on the given slopes S and flow depths H of the bedrock rivers, we then calculated transportable median grainsizes, D_{50}, and related effective impact energies, ε_{kin}, following the total load model procedure described above. The predicted D_{50} mostly exceeded reported D_{50}, but were consistent with maximum observed boulder sizes, D_{max}, which already move under partial submergence (Carling et al., 2002; Fujioka et al., 2015; Alexander and Cooker, 2016). Using the rock tensile strengths, σ_t, we obtained potential bedrock abrasion volumes V_a for the D_{50} grains by means of the extended erosivity regression (Fig. 3). Considering mean kinetic impact energy densities (ε_{kin} / D_{50}^2) and the assumed threshold for the onset of macro-abrasion (Fig. 2C), we then assigned the river sections to fall into the wear- and macro-abrasion regimes, respectively (Fig. 4).

GSA DATA REPOSITORY FIGURES AND TABLES

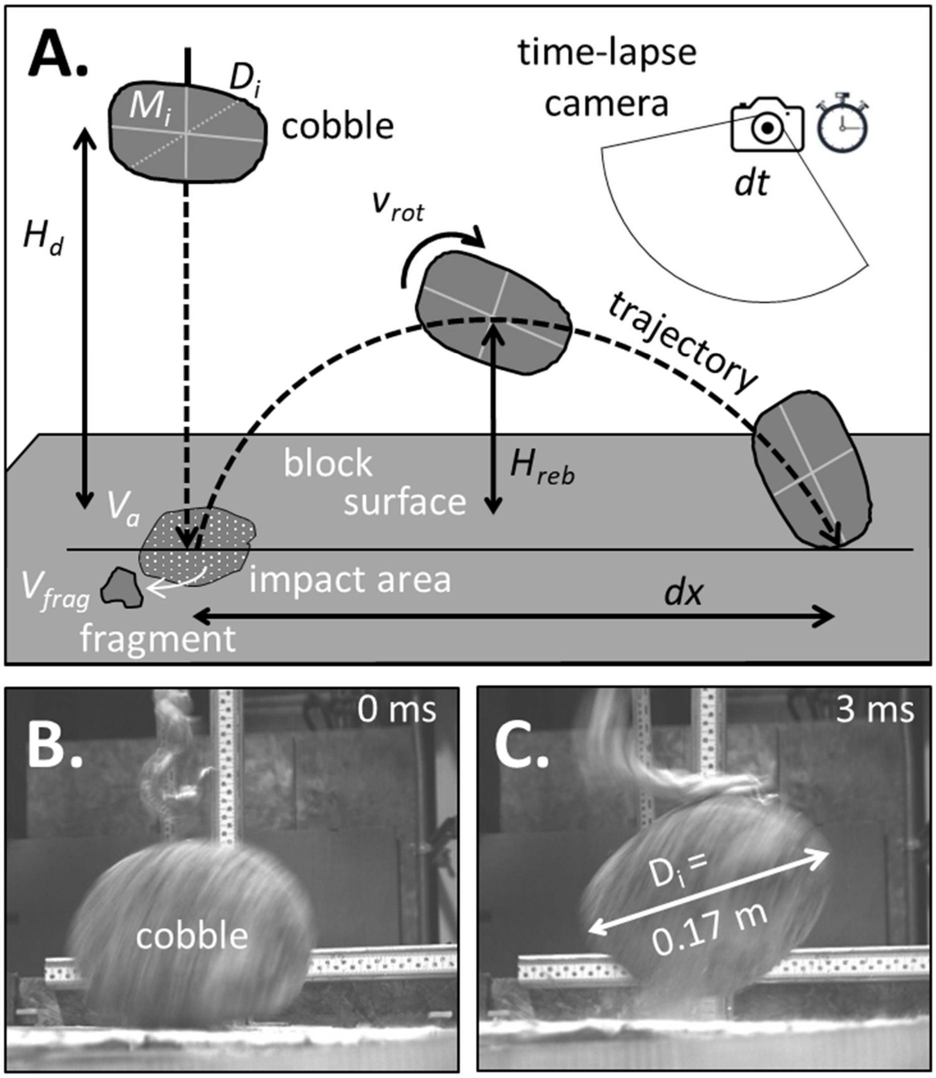

Figure S1. Impactor trajectory measurements shown for a dropped cobble (cf. Fig. 1B) with (A) definitions of the measured impactor values (mass M_i, diameter D_i, drop height H_d, rebound height H_{reb}, rebound rotation velocity $v_{rot,reb}$, hop distance dx and hop time dt), block abrasion volume V_a and fragment abrasion volume V_{frag}, and (B-C) time-lapse snapshots in microseconds of a cobble before and after its impact on a block's surface.

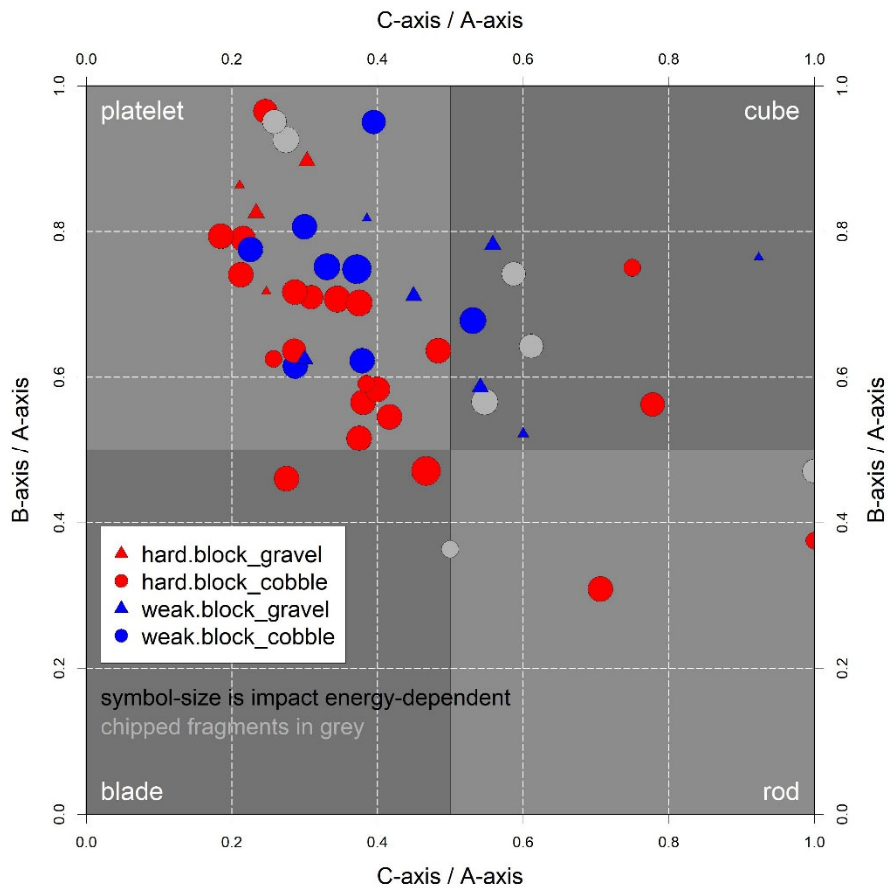

Figure S2. Size relations of the largest fragments abraded per impact experiment, shown in the framework of grain shape types (represented by four sectors with mainly platelet, cube, blade or rod shape). Defining their ABC-axis by decreasing lengths, most abraded fragments were of platelet-shape with size relations of C-axis/A-axis smaller than 0.5 and B-axis/A-axis larger than 0.5.

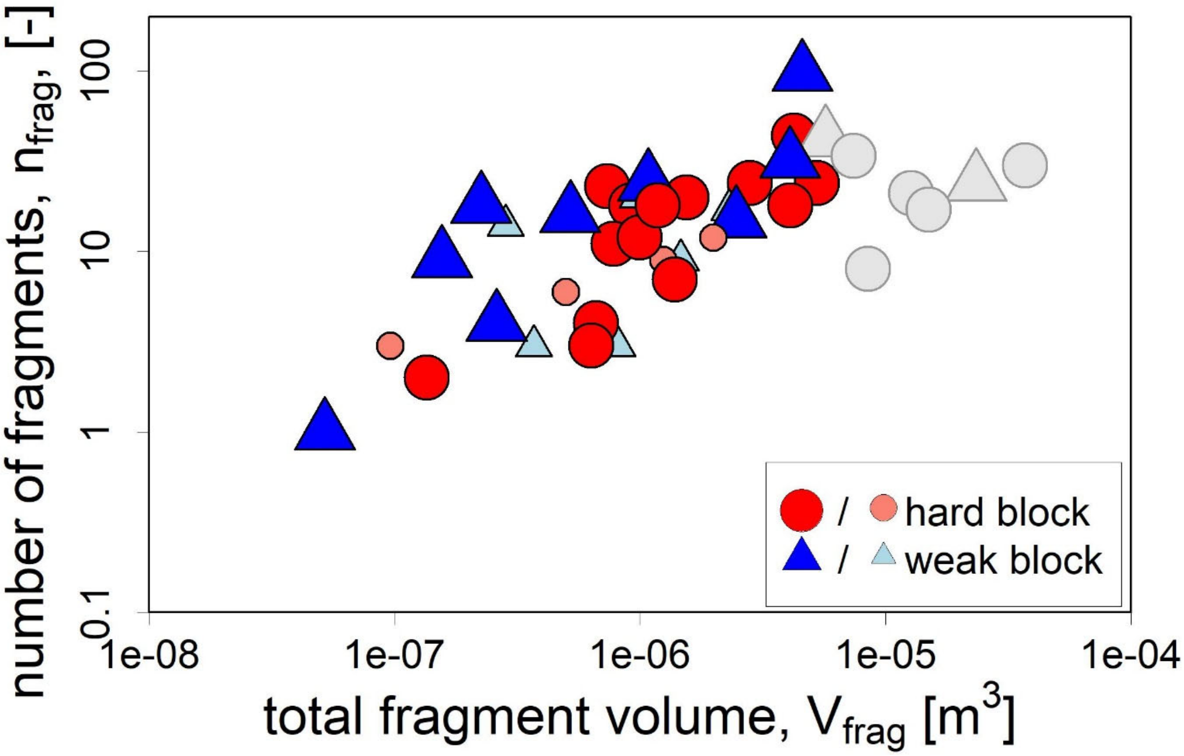

Figure S3. The increase in total fragment volume, V_{frag}, for higher impact energies was due to an increase of the number of fragments, n_{frag}, independent of the impactor size (represented by small and large symbols) or target strength (represented by color). Light grey-shaded symbols show chipped fragments.

Table S1. Overview of the macro-abrasion drop experiments. Individual runs during all seven experimental sets equal the number of structure from motion, *SfM*, models (62). Grey-shaded background denote variables hold constant and bold numbers show varied variables of impactor type (cobble versus pebbles), impactor mass, M_i, and impactor drop height, H_d (Fig. S1A). The tensile strengths, σ_t, of the concrete blocks (conditioned by their cement to sand mixture ratio) was measured using a Split-Hopkinson pressure bar and conform to published values of the same artificial rock material (Sklar and Dietrich, 2001).

	target		impactor(s)			runs		
exp. set	**casting ratio cement : sand**	**tensile strength τ [Mpa]**	**type**	**single mass M_i [kg]**	**drop height H_d [m]**	**impacts frequency**	**repetitions**	**no. of SfM models**
1	1 : 2 (hard)	2.34	cobble	11.8	***0.50 - 1.50***	1	3	12
2					***0.50 - 4.87***	5 (1)	1	8
3			pebbles	***0.3 - 0.5***	2.40		2	4
4	1 : 4 (weak)	1.32	cobble	11.8	***0.10 - 4.87***		1	13
5			pebbles	***0.1 - 0.5***	2.40			7
6				0.3		24	3	3
7				***0.3 - 0.5***		21	1	4

constant value ***varied value***

Table S2. Reported bedrock abrasion experiment data sets with calculated magnitudes of effective single grain impact energies, ε_{kin}, and abraded target volumes, V_a. The diameter $D_{ero,sphere}$ of equivalent abraded spheres with volume V_a is given for illustration, only.

experiments			orders of magnitudes for single grain impacts				
impactor	**target**	**test principle**	**impactor mass** M_i **[kg]**	**kinetic impact energy** ε_{kin} **[J]**	**abraded target volume** V_a **[m^3]**	**diameter of equiv. sphere with** V_a $D_{ero,sphere}$ **[m^3]**	**source**
Crystolon dust	plate glass	sand blasting	1e-9	1e-7 to 1e-8	1e-16 to 1e-15	1e-5	Head and Harr, 1970
steel balls	concretes with varying aggregates	abrasion mill	1e-3 to 1e-2	1e-3	1e-13 to 1e-12	1e-4 to 1e-5	Liu, 1981
sand, pebbles	natural rocks, artificial sandstone	abrasion mill	1e-7 to 1e-2	1e-9 to 1e-2	1e-18 to 1e-11	1e-6 to 1e-4	Sklar and Dietrich, 2001
pebbles	artificial sandstone	grain drop	1e-2	1e-1	1e-9	1e-3	Sklar and Dietrich, 2004
sand, pebbles	polyurethane foam	abrasion mill	1e-7 to 1e-1	1e-11 to 1e-2	1e-19 to 1e-11	1e-7 to 1e-4	Scheingross et al., 2014
pebbles, cobble	artificial sandstone	grain drop	1e-1 to 1e1	1e0 to 1e2	1e-7 to 1e-5	1e-3 to 1e-2	this study

Table S3. Compiled set of published bedrock river data (slope *S*, water depth *H*, measured grain sizes *D*, and partially rock tensile strength σ_t) and predicted values of potential streamflow erosivity, sorted by year of publication and order in the original publication. Note several sections per listed rivers and partly converted or assumed tensile strengths.

REFERENCES CITED

AgiSoft PhotoScan Professional (Version 1.4.5; Software), 2018: retrieved from http://www.agisoft.com/downloads/installer/

Alexander, J., and Cooker, M.J., 2016, Moving boulders in flash floods and estimating flow conditions using boulders in ancient deposits: Sedimentology, v. 63, p. 1582-1595, https://doi.org/10.1111/sed.12274

Alho, P., Russel, A.J., Carrivick, J.L., and Kaeyhkoe, J., 2005, Reconstruction of the largest Holocene joekulhlaup within Joekulsa a Fjoellum, NE Iceland: Quaternary Science Reviews, v. 24, p. 2319-2334, https://doi.org/10.1016/j.quascirev.2004.11.021

Baker, V.R. and Pickup, G., 1987, Flood geomorphology of the Katherine Gorge, Northern Territory, Australia, GSA Bulletin, v. 98, p. 635-646, https://doi.org/10.1130/0016-7606(1987)98<635:FGOTKG>2.0.CO;2

Baker, V.R. and Kale, V.S., 1998, The Role of Extreme Floods in Shaping Bedrock Channels, *in* Tinkler, K.J., and Wohl, E.E., eds., Rivers Over Rock: Fluvial Processes in Bedrock Channels: American Geophysical Union Geophysical Monograph 107, p. 153-165, https://doi.org/10.1029/GM107p0153

Carling, P.A., Hoffmann, M., and Blatter, A.S., 2002, Initial Motion of Boulders in Bedrock Channels, *in* House, P.K., Webb, R.H., Baker, V.R., and Levish, D.R., eds, Ancient Floods, Modern Hazards, American Geophysical Union Water Science and Application, v. 5, p. 147-160, https://doi.org/10.1029/WS005p0147

CloudCompare (version 2.11; GPL software), 2019: retrieved from http://www.cloudcompare.org

Farin, M., Mangeney, A., de Rosny, J., Toussaint, R., Sainte-Marie, J., and Shapiro, N.M., 2016, Experimental validation of theoretical methods to estimate the energy radiated by elastic waves during an impact: Journal of Sound and Vibration, v. 362, p. 176-202, https://doi.org/10.1016/j.jsv.2015.10.003

Fernandez Luque, R., and van Beek, R., 1976, Erosion and transport of bed-load sediment: Journal of Hydraulic Research, v. 14 (2), p. 127– 144, https://doi.org/10.1080/00221687609499677

Fujioka, T., Fink, D., Nanson, G., Mifsud, C., and Wende, R., 2015, Flood-flipped boulders: In-situ cosmogenic nuclide modeling of flood deposits in the monsoon tropics of Australia: Geology, v.43 (1), p. 43-46, https://doi.org/10.1130/G35856.1

Jamshidi, A., Yazarloo, R., and Gheiji, S., 2018, Comparative evaluation of Schmidt hammer test procedures for prediction of rock strength: International Journal of Mining and Geo-Engineering, v. 52 (2), p. 199-206, https://doi.org/10.22059/ijmge.2018.244154.594702

Lamb, M.P., Dietrich, W.E., and Venditti, J.G., 2008b, Is the critical Shields stress for incipient sediment motion dependent on channel-bed slope?: Journal of Geophysical Research, v. 113, F02008, https://doi.org/10.1029/2007JF000831

Neilson, J.H. and Gilchrist, A., 1968, Erosion by a stream of solid particles: Wear, v. 11 (2), p. 111-122, https://doi.org/10.1016/0043-1648(68)90591-7

Parker, G., 1978, Self-formed straight rivers with equilibrium banks and mobile bed. Part 2. The gravel river: Journal of Fluid Mechanics, v. 89 (1), p. 127– 146, https://doi.org/10.1017/S0022112078002505

Zhou, Y.X., Xia, K., Li, X.B., Li, H.B., Ma, G.W., Zhao, J., Zhou, Z.L., and Dai, F., 2011, Suggested Methods for Determining the Dynamic Strength Parameters and Mode-I Fracture Toughness of Rock Materials, *in* Ulusay, R., eds, The ISRM Suggested Methods for Rock Characterization, Testing and Monitoring: 2007–2014. Springer, Cham, p. 35-44, https://doi.org/10.1007/978-3-319-07713-0_3